RSC Advances

ROYAL SOCIETY OF CHEMISTRY

www.rsc.org/advances

Journal Name

ARTICLE

High performance supercapacitor under extremely low environmental temperature

Received 00th January 20xx,
Accepted 00th January 20xx

DOI: 10.1039/x0xx00000x

www.rsc.org/

Yue Zhou[a,1], Mehdi Ghaffari[b,1], Minren Lin[b], Haiping Xu[c], Huaqing Xie[c], Chong Min Koo[d], Q. M. Zhang[a,b*]

Supercapacitors with broad operation temperature range, especially with capability of operating at low temperature (below -50 °C), are required for the applications in extreme environments. This paper presents a high performance supercapacitor, consisting of highly aligned nano-porous graphene (A-NPG) with an eutectic mixture of ionic liquids (ILs) 1-butyl-4-methylpyridinium tetrafluoroborate ($BMPBF_4$) in 1-butyl-3-methylimidazolium tetrafluoroborate ($BMIBF_4$), which exhibits a high capacitance performance over a temperature range from – 50 °C to 80 °C. The experimental results reveal a reducing of melting temperature T_m of the eutectic mixture to – 74 °C, compared with -39 °C of $BMIBF_4$. The increased ionic conductivity and reducd T_m of the eutectic mixture, combined ultrahigh density A-NPG electrodes, enable the supercapacitor to show a high capacitance of 125 F cm^{-3} at room temperature and 106 F cm^{-3} at – 50 °C. In contrast, the supercapacitor with pure $BMIBF_4$ shows a capacitance of 119 F cm^{-3} and 16.5 F cm^{-3} at room temperature and – 50 °C, respectively.

1. Introduction

Supercapacitors are a class of energy storage devices which store charges at the interface between electrode and electrolyte [1-6]. They have found wide applications in electrical and hybrid electrical vehicles, portable electronic devices and backup power sources due to their much higher power density and cycle life compared with batteries and higher energy density than the dielectric capacitors [4, 7-14]. However, the relatively narrow operation temperature range of the supercapacitors limit their applications in extreme environments such as space applications where the energy storage devices are required to operate at wide temperature range, especially at temperatures below -40 °C [15-18]. At low temperatures, the very low conductivity of electrolyte will hinder ion transport which influences the ions absorption/desorption for electrical double layer capacitors and inhibits the faradic reactions for batteries and pseudocapacitors [19-21].

Ionic liquids (ILs) are superior electrolytes that offer large electrochemical stability range (up to 6 V) in addition to the high thermal and environmental stability, low melting point and high ion conductivity [22-26]. In the last few years, it was found that the eutectic mixtures of ionic liquids could be employed to broaden the operation temperature and increase the ionic mobility at lower temperatures compared to the individual ionic liquids [27, 28]. In most ionic liquids, it was shown that the crystallization process is mainly through the anion ordering. In case the cations can prevent the ordering of the anions such as in a proper eutectic mixture of ILs, the gelation and solidification of the mixture can be shifted to lower temperatures. Although there have been several studies on the eutectic mixtures of ionic liquid for energy storage applications, these mixtures are mainly based on piperidinium (PIP) and pyrrolidinium (PYR) cations which have very large viscosity and low conductivity (~0.5 S m^{-1} at room temperature) [29-31]. Hence, the electrochemical properties of devices were partially sacrificed.

In this work, a novel eutectic electrolyte system based on 1-butyl-3-methylimidazolium tetrafluoroborate ($BMIBF_4$) with relatively high conductivity (~5 S m^{-1}) and 1-butyl-4-methylpyridinium tetrafluoroborate ($BMPBF_4$) was prepared and investigated. These ILs have the same anions; whereas, BMI ($C_8H_{15}N_2$) is an imidazolium cation while BMP ($C_{10}H_{16}N$) is a pyridinium cation. These two cations have relatively similar structures and side chains with similar values of molecular weights ($BMIBF_4$: 226.02 and $BMPBF_4$: 237.05). It was hypothesized that this slight difference in the cation structures will inhibit the ordering arrangement of the anions and hence will reduce the melting point while enhancing the ionic conductivity of the eutectic mixture.

Recently, many works have been devoted to fabricate novel graphene materials for the applications in electrochemical storage field due to their high specific surface area and high conductivity [12, 14]. However, so far only few studies have been conducted to investigate the performance of supercapacitor cells based on graphene under extreme conditions. In this work, a vacuum assisted self-assembly method was used to fabricate highly aligned nanoporous graphene (A-NPG) with the density as high as 1.15 g cm^{-3}. Meanwhile, the uniform micropores are created in the A-NPG fabricated based on this method [32]. The

[a] Department of Electrical Engineering, Pennsylvania State University, University Park, Pennsylvania 16802, USA.
*Corresponding author. Email address: qxz1@psu.edu

[b] Department of Materials Science and Engineering, Pennsylvania State University, University Park, Pennsylvania 16802, USA.
[c] School of Environmental and Materials Engineering, Shanghai Second Polytechnic University, Shanghai 201209, China.
[d] Center for Materials Architecturing, Korea Institute of Science and Technology (KIST), Hwarangno 14-gil 5, Soengbuk-gu, Seoul 136-791, Republic of Korea.
[1]These authors contributed equally to this work.

high density and uniform pore size lead to the high volumetric performance and enhance the ion transport.

Here, we show that employing the eutectic mixture of $BMIBF_4$ and $BMPBF_4$ enables the supercapacitor cell perform well at a wide temperature range (from -60 °C to 80 °C). The A-NPG supercapacitor with the eutectic mixture of $BMIBF_4$ and $BMPBF_4$ shows a room temperature specific capacitance of 125 F cm^{-3} (109 F g^{-1}) while at -50 °C, the cell still maintains a specific capacitance of 106 F cm^{-3} (92 F g^{-1}), which is 85% of the room temperature capacitance. In contrast, the capacitance of the cells with $BMIBF_4$ as the electrolyte drops from the room temperature value of 119 F cm^{-3} (103 F g^{-1}) to 16.5 F cm^{-3} (14 F g^{-1}) at -50 °C, which is about 14% of the room temperature capacitance.

2. Experimental

2.1. Preparation of $(BMIBF_4)_{0.5}(BMPBF_4)_{0.5}$ eutectic mixture

$BMIBF_4$ and $BMPBF_4$ were purchased from Iolitech Inc. Prior to mixing, the two electrolytes were heated at 100 ºC in a vacuum oven for more than 2 weeks in order to remove any trace amount of water. The eutectic mixture of $(BMIBF_4)_{0.5}(BMPBF_4)_{0.5}$ was prepared by mixing equal amounts of these ionic liquids in the glove box under a nitrogen atmosphere, and then was stirred for one day under the nitrogen to ensure of uniform blending. After that, the mixture was collected and stored in a vacuum oven at 100 ºC for future use. The final eutectic mixture was a clear light brown fluid. DSC measurements were carried out from -90 ºC to 30 ºC using a TA Instrument differential scanning calorimeter model Q2000 with liquid nitrogen cooling for the pure ILs and the mixtures. The scan rate was 5 ºC/min and the sample pans were all aluminum with the capability of hermetic sealing.

2.2. Preparation of ultra-high density highly aligned nano-porous graphene electrodes

The nanoporous graphene was prepared by activation of graphite oxide via a technique that has been reported before [32, 33]. The vacuum-assisted self-assembly method was applied to produce ultrahigh density of the nanoporous graphene electrodes. Firstly, the nanoporous graphene powder was dispersed in N,N-dimethylformamide (DMF, Aldrich) with the help of sonicator and the mixture was vacuum filtered with an Anodisc filter membrane (Whatman, 25 mm diameter with 0.02 μm pore size). After filtration, the highly aligned nanoporous graphene (A-NPG) electrode film and membrane were put in KOH aqueous solution for 1 hour to dissolve the Anodisc membrane. The A-NPG sheet floated on the surface of this solution. Finally, the A-NPG electrode was air dried for 2 h and vacuum dried at 100 °C for 24 h before use.

2.3. Fabrication and characterization of graphene supercapacitor cell with different electrolytes

The A-NPG electrode (100 μm thick) was attached on gold film which serves as the current collector. The supercapacitor cell was assembled by assembling two symmetric A-NPG electrodes, separated by a 25 μm thick porous membrane (Celgard 3501, Celgrad LLC) while pure ILs and mixture ILs were used as electrolyte, respectively. The electrical impedances were characterized using a potentiostat/frequency analyzer (Parstat 2273). CV curve measurements were carried out at different scan rates with Versastat 4 (Princeton Applied Research). The specific capacitance was calculated from the integration of discharge area of CV curve, versus the potential, scan rate and total mass of electrodes, and multiplied by 4. The equation is shown in the supporting information.

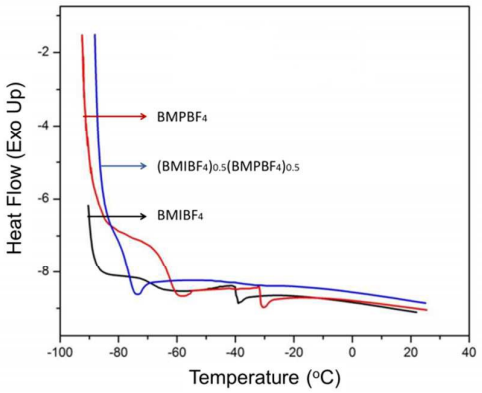

Figure 1. DSC curves of $BMIBF_4$, $BMPBF_4$, and $(BMIBF_4)_{0.5}(BMPBF_4)_{0.5}$ eutectic mixture.

3. Results and discussion

The melting temperatures T_m of individual ILs and eutectic mixture of the ILs were studied by differential scanningcalorimetry (DSC) over a wide temperature range. The DSC data in Figure 1 shows that the melting temperature T_m of $BMPBF_4$ is at -30 ºC, and the T_m of $BMIBF_4$ is observed at -39 ºC. This difference could be attributed to the more flat and symmetric structure of BMP cation than that of BMI that results in easier packing and hence higher melting temperature for this electrolyte. There are additional solid-solid transitions for these ionic liquids that take place at temperatures below their melting points (-58 ºC for $BMPBF_4$ and -77 ºC for $BMIBF_4$), possibly due to recrystallization or glass transition for these electrolytes [34, 35]. In contrast, the melting of the eutectic mixture occurs at -74 °C. There is no solid-solid transition process observed in the mixture to -90 ºC. These results indicate that blending $BMPBF_4$ with $BMIBF_4$ reduces the melting temperature of the mixture significantly which could be a direct result of the dimensional mismatch between the cations in the two ILs that impedes the formation of crystallites in the mixture. The lowering of the melting temperature broadens the operation temperature range of the electrolytes to below – 50 °C.

Figure 2a and Figure 2b exhibit the SEM images of highly aligned morphology for porous graphene sheets based on vacuum-assisted self-assembly method with top and cross-sectional view, respectively. It is obvious that the efficient successive packing of graphene sheets is taking place while concentration and distribution of nano-sized pores are preserved, which will enhance the ion distribution in the energy

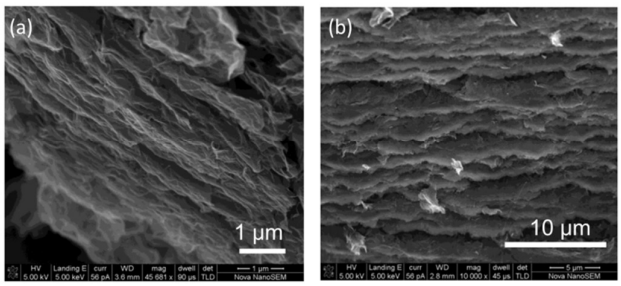

Figure 2. SEM image of the highly-aligned nanoporous graphene electrode with (a) top and (b) cross-sectional view.

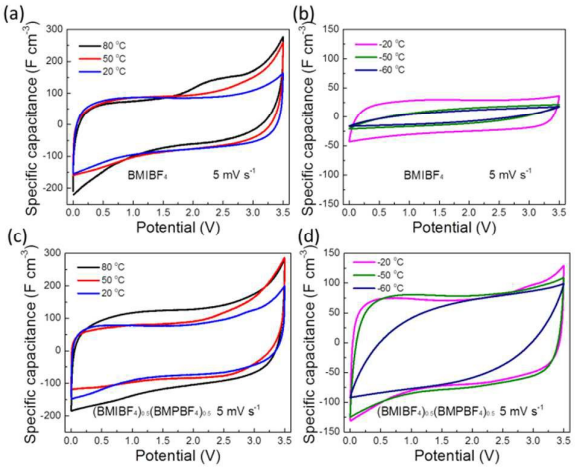

Figure 3. CV curves for the cells with $BMIBF_4$ as the electrolyte with the scan rates of 5 mV s^{-1} at (a) above and (b) below 0 °C. CV curves for the cells with $(BMIBF_4)_{0.5}(BMPBF_4)_{0.5}$ as the electrolyte at scan rates of 5 mV s^{-1} at (c) above and (d) below 0 °C

storage system. The supercapacitor cell was assembled by vertically placing two symmetric graphene sheets as electrodes, separated by a 25 μm thick porous membrane (Celgard 3501, Celgrad LLC) while pure ILs and mixture ILs were used as electrolyte, respectively.

Cyclic voltammetry (CV) measurements were performed to investigate the electrochemical behavior of the cell with the eutectic ILs electrolyte system. The experiments were conducted at the temperature range from -60 ºC to 80 ºC. At each interval, the system was allowed to equilibrate for at least two hours inside the chamber to eliminate the hysteresis from previous experiments. Figure 3 shows the comparison of CV curves for A-NPG electrodes with pure $BMIBF_4$ and $(BMIBF_4)_{0.5}(BMPBF_4)_{0.5}$ electrolytes, at different temperatures and 5 mV s^{-1}. The capacitor cells with pure ILs exhibit near ideal capacitive behavior, i.e., nearly rectangular CV curves, at temperatures above 20 °C, as shown in Figure 3a. Some deviation from the rectangular shape CV curves observed at 50 ºC and 80 ºC can be related to chemical reactions in the system at higher temperatures under high operation voltages. However, the capacitance value diminishes greatly at temperatures below 0 °C as shown in Figure 3b. This could be attributed to the fast diminishing conductivity of this electrolyte at lower temperatures despite its lower melting temperature. In other words, although the electrolyte is still liquid state at temperatures above T_m (~ - 39 ºC), the high viscosity of the electrolyte (due to gelation before freezing) does not allow the ions to propagate in the porous electrodes during the charge/discharge cycle and consequently the capacitance reduces significantly.

On the other hand, the capacitor cells with the eutectic mixture exhibit very different low temperature behavior, as shown in Figures 3c and 3d. Firstly, in the whole temperature range investigated, the cells with the eutectic mixture have larger specific capacitance than that with the single IL. For instance, at 80 °C and 5 mV s^{-1} scan rate, the specific capacitance with mixture electrolyte is 158 F cm^{-3} while with pure ILs, the capacitance is 130 F cm^{-3}. This is a direct consequence of the higher mobile ion concentration and ionic

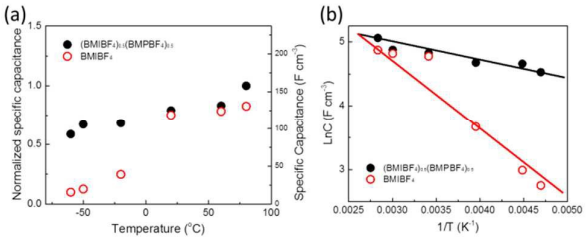

Figure 4. (a) Comparison of the normalized capacitances of cells with the $BMIBF_4$ (open circles) and with $(BMIBF_4)_{0.5}(BMPBF_4)_{0.5}$ (filled circles) vs. temperature from -60 °C to 80 °C. (b) Arrhenius plot of cells with the two electrolytes.

conductivity of the eutectic mixture electrolyte compared to the single IL. Secondly, the capacitor cells with the eutectic mixture exhibit near square CV curves at temperatures to -50 ºC, which is attributed to the improved conductivity of the electrolyte at lower temperatures besides the lowering of T_m to –74 ºC.

As a comparison, Figure 4a presents the capacitance changes in the operating temperature range between the capacitor cells with $BMIBF_4$ and $(BMIBF_4)_{0.5}(BMPBF_4)_{0.5}$ as electrolytes, respectively, extracted from CV curves in Figure 3 (at 5 mV s^{-1} scan rate). The capacitances are normalized for a better comparison. As has been shown above, the capacitance of the cell with eutectic mixture is larger than that with $BMIBF_4$ in the whole temperature range, especially in the sub-zero range. This indicates that the ions transportation in the eutectic mixture electrolyte is much higher in the whole temperature range, especially at sub-zero temperatures, to generate a high capacitance of the cell. Moreover, the cell with eutectic mixture electrolyte shows much better capacitance retention as the temperature is reduced from room temperature to -60 °C (more than 80% retention) compared with the cell with pure $BMIBF_4$ as electrolyte. The cell with eutectic mixture exhibits volumetric capacitances of 106 F cm^{-3} and 94 F cm^{-3} at -50 °C and -60 °C, respectively. As a comparison, at – 50 °C, the cell with pure $BMIBF_4$ as electrolyte retains 14% of the room temperature capacitance. The large difference in capacitance retention is due to the improved conductivity of the eutectic mixture electrolyte at low temperatures. Therefore, the eutectic mixture electrolyte system enables the cell electrodes to deliver large amount of charges at very low temperatures where the conventional supercapacitors are unable to perform. In order to study the influence of the two electrolytes on the supercapacitor cells with different temperatures, the Arrhenius plot based on specific capacitance versus inverse temperature was investigated. The motion of ions is highly related to the double layer charge formation and dissipation at the interface between electrode and electrolyte. The kinetic involved can be represented by an Arrhenius-type equation: $\boldsymbol{Q = Q_0 \exp(-E_a/RT)}$ or $\boldsymbol{C = C_0 \exp(-E_a/RT)}$, where $\boldsymbol{Q}$ is the accumulated charges at the interface, $\boldsymbol{Q_0}$ is the pre-exponential factor, $\boldsymbol{E_a}$ is the activation energy, $\boldsymbol{R}$ is the universal gas constant, $\boldsymbol{T}$ is the absolute temperature, $\boldsymbol{C}$ is the specific capacitance and $\boldsymbol{C_0}$ is the pre-exponential capacitance constant. The equation $\boldsymbol{InC = InC_0 - E_a/RT}$ can be derived from the equation above. Hence, the activation energy is obtained from the slope ($\boldsymbol{-E_a/R}$) of Arrhenius plot. Based on the Figure 4b, the activation energy of cells using $BMIBF_4$ and $(BMIBF_4)_{0.5}(BMPBF_4)_{0.5}$ as electrolytes are 2.11 and 0.57 kcal/mol, respectively. The activation energy based on the new eutectic electrolyte is much

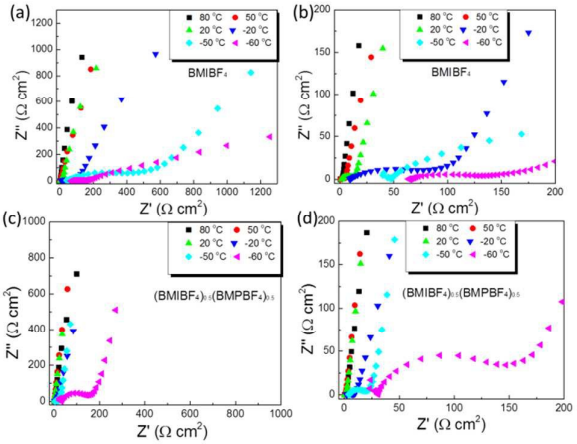

Figure 5. Nyquist plots of the cells with $BMIBF_4$ electrolyte in the (a) whole frequency range, (b) high frequency range (expanded view). Nyquist plots of the cells with $(BMIBF_4)_{0.5}(BMPBF_4)_{0.5}$ electrolyte in the (c) whole frequency range, (d) high frequency range (expanded view). The data were collected in temperatures from – 60 °C to 80 °C.

lower compared with other supercpacitor systems, exhibiting a better performance of the formation and dissociation of the double layers [36, 37].

The electrochemical performance for the newly developed eutectic mixture was further studied by impedance analysis. Figure 5 compares the Nyquist plots between the cells with $BMIBF_4$ and with $(BMIBF_4)_{0.5}(BMPBF_4)_{0.5}$ mixture. Consistent with the data from the CV curves in Figure 3, the cells with $BMIBF_4$ show a relatively small series resistance at temperatures above 20 ºC (7.2 Ω cm^2 at 20 ºC to 2.8 Ω cm^2 at 80 ºC), where the vertical increase in the imaginary part of impedance provides evidence of the ideal capacitive behavior in the high temperatures [38]. On the other hand, the size of the semi-circle at high frequency region increases significantly at sub-zero temperatures, as shown in Figure 5b, indicating an increased equivalent series resistance (ESR) of the cell. This is related to the low conductivity of the $BMIBF_4$ electrolyte and possible gelation in this system at sub-zero temperatures.

For the eutectic mixture electrolyte, the Nyquist plots of Figures 5c and 5d show a remarkable reduction in the series resistance, compared with Figures 5a and 5b, and the ideal capacitive behavior can be observed in the whole temperature range. Although the size of the semi-circle at high frequency region increases at low temperatures, the ESR values are still small, e.g., 1.9 Ω cm^2 at 20 ºC and 4.7 Ω cm^2 at -50 ºC. Consistent with the results from the CV curves, the smaller ESR in the cells with the eutectic mixture is a direct consequence of the improved ionic conductivity in the electrolytes. The impedance data of the cell with eutectic mixture shows a large increase in ESR at – 60 °C (Figure 5d) which could be related to the possible gelation in the electrolyte system, causing a reduction of the cell capacitance.

4. Conclusions

In this work, a supercapacitor with a novel eutectic mixture electrolyte system of $(BMIBF_4)_{0.5}(BMPBF_4)_{0.5}$ was fabricated and investigated. It was shown that the slight difference in the cation structure of the two ILs inhibits the ordering arrangement of the anions and crystallization process. Hence, the temperatures of gelation and solidification of the mixture electrolyte were lowered so that the supercapacitor can operate at a wide temperature range from -50 °C to 80 °C. The supercapacitor with the eutectic mixture shows a capacitance of 125 F cm^{-3} at room temperature and 106 F cm^{-3} at – 50 °C, compared with 119 F cm^{-3} and 16.5 F cm^{-3} at the same temperatures for the cell with pure $BMIBF_4$. Overall, the unique eutectic mixture ILs system combined with ultrahigh density aligned nanoporous graphene electrodes provides a promising candidate for energy storage applications at extreme conditions such as for aerospace applications.

Acknowledgements

This work was supported by AFOSR under Grant No. FA9550-11-1-0192 and NSF under Grant No. CMMI-1130437.

Notes and references

1. Y. Gogotsi and P. Simon, *Science*, 2011, **334**, 917-918.
2. P. Simon, Y. Gogotsi and B. Dunn, *Science*, 2014, **343**, 1210-1211.
3. Y. Wang, Z. Shi, Y. Huang, Y. Ma, C. Wang, M. Chen and Y. Chen, *J. Phys. Chem. C*, 2009, **113**, 13103-13107.
4. D. Pech, M. Brunet, H. Durou, P. Huang, V. Mochalin, Y. Gogotsi, P.-L. Taberna and P. Simon, *Nat. Nanotechnol.*, 2010, **5**, 651-654.
5. C. Merlet, B. Rotenberg, P. A. Madden, P.-L. Taberna, P. Simon, Y. Gogotsi and M. Salanne, *Nat. Mater.*, 2012, **11**, 306-310.
6. Y. Zhou, N. Lachman, M. Ghaffari, H. Xu, D. Bhattacharya, P. Fattahi, M. R. Abidian, S. Wu, K. K. Gleason and B. L. Wardle, *J. Mater. Chem. A*, 2014, **2**, 9964-9969.
7. F. Zhang, T. Zhang, X. Yang, L. Zhang, K. Leng, Y. Huang and Y. Chen, *Energy Environ. Sci.*, 2013, **6**, 1623-1632.
8. Y. Zhou, H. Xu, N. Lachman, M. Ghaffari, S. Wu, Y. Liu, A. Ugur, K. K. Gleason, B. L. Wardle and Q. Zhang, *Nano Energy*, 2014, **9**, 176-185.
9. T. Takamura, Y. Sato and Y. Sato, *J. Power Sources*, 2011, **196**, 5774-5778.
10. A. Izadi-Najafabadi, S. Yasuda, K. Kobashi, T. Yamada, D. N. Futaba, H. Hatori, M. Yumura, S. Iijima and K. Hata, *Adv. Mater.*, 2010, **22**, E235-E241.
11. M. Ghaffari, S. Kosolwattana, Y. Zhou, N. Lachman, M. Lin, D. Bhattacharya, K. K. Gleason, B. L. Wardle and Q. Zhang, *Electrochim. Acta*, 2013, **112**, 522-528.
12. P. Simon and Y. Gogotsi, *Nat. Mater.*, 2008, **7**, 845-854.
13. G. Xiong, C. Meng, R. G. Reifenberger, P. P. Irazoqui and T. S. Fisher, *Electroanalysis*, 2014, **26**, 30-51.
14. G. Xiong, C. Meng, R. G. Reifenberger, P. P. Irazoqui and T. S. Fisher, *Advanced Energy Materials*, 2014, **4**.
15. K. Hung, C. Masarapu, T. Ko and B. Wei, *J. Power Sources*, 2009, **193**, 944-949.
16. R. Kötz, M. Hahn and R. Gallay, *J. Power Sources*, 2006, **154**, 550-555.
17. C. Yuan, X. Zhang, Q. Wu and B. Gao, *Solid State Ionics*, 2006, **177**, 1237-1242.
18. P. Liu, M. Verbrugge and S. Soukiazian, *J. Power Sources*, 2006, **156**, 712-718.

19. B. Conway, *Electrochemical supercapacitors: scientific fundamentals and technological applications (POD)*, Kluwer Academic/Plenum: New York, 1999.
20. C. R. Sides and C. R. Martin, *Adv. Mater.*, 2005, **17**, 125-128.
21. G. Xiong, A. Kundu and T. S. Fisher, *Journal*, 2015.
22. M. Galiński, A. Lewandowski and I. Stępniak, *Electrochim. Acta*, 2006, **51**, 5567-5580.
23. Y. Zhou, M. Ghaffari, M. Lin, E. M. Parsons, Y. Liu, B. L. Wardle and Q. Zhang, *Electrochim. Acta*, 2013, **111**, 608-613.
24. L. Zhao, Y. S. Hu, H. Li, Z. Wang and L. Chen, *Adv. Mater.*, 2011, **23**, 1385-1388.
25. A. Balducci, R. Dugas, P.-L. Taberna, P. Simon, D. Plee, M. Mastragostino and S. Passerini, *J. Power Sources*, 2007, **165**, 922-927.
26. M. Ghaffari, W. Kinsman, Y. Zhou, S. Murali, Q. Burlingame, M. Lin, R. Ruoff and Q. Zhang, *Adv. Mater.*, 2013, **25**, 6277-6283.
27. M. Kunze, S. Jeong, E. Paillard, M. Winter and S. Passerini, *J. Phys. Chem. C*, 2010, **114**, 12364-12369.
28. M. Kunze, M. Montanino, G. B. Appetecchi, S. Jeong, M. Schonhoff, M. Winter and S. Passerini, *J. Phys. Chem. A*, 2010, **114**, 1776-1782.
29. P. Johansson, L. E. Fast, A. Matic, G. B. Appetecchi and S. Passerini, *J. Power Sources*, 2010, **195**, 2074-2076.
30. S. Zhang, N. Sun, X. He, X. Lu and X. Zhang, *J. Phys. Chem. Ref. Data*, 2006, **35**, 1475-1517.
31. W.-Y. Tsai, R. Lin, S. Murali, L. L. Zhang, J. K. McDonough, R. S. Ruoff, P.-L. Taberna, Y. Gogotsi and P. Simon, *Nano Energy*, 2013, **2**, 403-411.
32. M. Ghaffari, Y. Zhou, H. Xu, M. Lin, T. Y. Kim, R. S. Ruoff and Q. Zhang, *Adv. Mater.*, 2013, **25**, 4879-4885.
33. Y. Zhu, S. Murali, M. D. Stoller, K. Ganesh, W. Cai, P. J. Ferreira, A. Pirkle, R. M. Wallace, K. A. Cychosz and M. Thommes, *Science*, 2011, **332**, 1537-1541.
34. R. Palm, H. Kurig, K. Tõnurist, A. Jänes and E. Lust, *Electrochem. Commun.*, 2012, **22**, 203-206.
35. R. Lin, P.-L. Taberna, S. Fantini, V. Presser, C. R. Pérez, F. Malbosc, N. L. Rupesinghe, K. B. Teo, Y. Gogotsi and P. Simon, *J. Phys. Chem. Lett.*, 2011, **2**, 2396-2401.
36. R. Vellacheri, A. Al-Haddad, H. Zhao, W. Wang, C. Wang and Y. Lei, *Nano Energy*, 2014, **8**, 231-237.
37. C. Liu, Z. Yu, D. Neff, A. Zhamu and B. Z. Jang, *Nano letters*, 2010, **10**, 4863-4868.
38. Q. Cheng, J. Tang, J. Ma, H. Zhang, N. Shinya and L.-C. Qin, *Carbon*, 2011, **49**, 2917-2925.

Table of contents

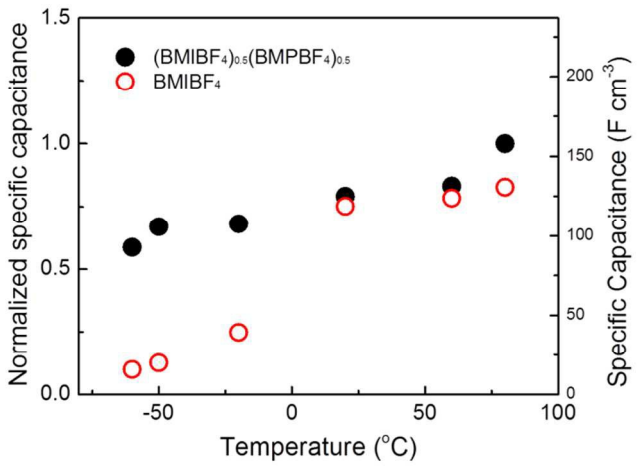

A supercapacitor cell, consisting of ultra-high density highly aligned nano-porous graphene electrodes with an eutectic mixture of ionic liquids $BMPBF_4$ in $BMIBF_4$ as electrolyte, exhibits a high capacitance performance over a temperature range from – 50 ^{o}C to 80 ^{o}C.